

Glycosylated Peptoid Nanosheets as a Multivalent Scaffold for Protein Recognition

Alessia Battigelli,¹ Jae Hong Kim,¹ Dilani C. Dehigaspitiya,² Caroline Proulx,¹ Ellen J. Robertson,¹ Daniel J. Murray,¹ Behzad Rad,¹ Kent Kirshenbaum,² and Ronald N. Zuckermann^{1*}

¹The Molecular Foundry, Lawrence Berkeley National Laboratory, 1 Cyclotron Road, Berkeley, California 94720, United States.

²Dept. of Chemistry, New York University, 100 Washington Square East, New York, New York 10003, United States.

ABSTRACT: Glycoproteins adhered on the cellular membrane play a pivotal role in a wide range of cellular functions. Their importance is particularly relevant in the recognition process between infectious pathogens (such as viruses, bacteria, toxins) and their host cells. Multivalent interactions at the pathogen-cell interfaces govern binding events and can result in a strong and specific interaction. Here we report an approach to mimic the cell surface presentation of carbohydrate ligands by the multivalent display of sugars on the surface of peptoid nanosheets. The constructs provide a highly organized 2D platform for recognition of carbohydrate-binding proteins. The sugars were displayed using different linker lengths or within loops containing 2 to 6 hydrophilic peptoid monomers. Both the linkers and the loops contained one alkyne-bearing monomer, to which different saccharides were attached by copper-catalyzed azide-alkyne cycloaddition reactions. Peptoid nanosheets functionalized with different saccharide groups were able to selectively bind multivalent lectins, Concanavalin A and Wheat Germ Agglutinin, as observed by fluorescence microscopy and a homogeneous FRET-based binding assay. To evaluate the potential of this system as sensor for threat agents, the ability of functionalized peptoid nanosheets to bind Shiga toxin was also studied. Peptoid nanosheets were functionalized with globotriose, the natural ligand of Shiga toxin, and the effective binding of the nanomaterial was verified by the FRET-based binding assay. In all cases, evidence for multivalent binding was observed by systematic variation of the ligand display density on the nanosheet surface. These cell surface mimetic nanomaterials may find utility in the inactivation of pathogens or as selective molecular recognition elements.

KEYWORDS: protein-mimetic materials, molecular recognition, multivalent binding, two-dimensional nanomaterials, bioinspired polymers, cell-surface mimetics.

In nature, multivalency is important for the selective binding of many receptors to their target molecules. The phenomenon has been shown to play a significant role in a variety of key biological processes, such as guest-host recognition, cellular adhesion, and signaling processing.^{1,2} One of the most relevant examples of multivalency in nature is the interaction between multivalent proteins and membrane-bound carbohydrates on the cell surface. The cell membrane is characterized by a diversity of glycoproteins and glycolipids that anchor an abundant heterogeneity of carbohydrates to the cell surface. Many infectious pathogens, such as virus and bacteria, specifically recognize their host cells through multivalent interactions with these sugars to start the infection process.^{3,4} The monovalent interaction of a carbohydrate with a protein is usually weak, with the overall binding avidity significantly enhanced when the sugars are displayed in a multivalent context, where the corresponding protein can interact with multiple sugars.

Many researchers have therefore attempted to synthesize mimics of the cell surface that display multivalent ligands, typically for the detection or inhibition of biological pathogens.⁵⁻⁷ For example, dendrimers,^{8,9} fullerenes,¹⁰ ro-

taxanes,¹¹ polymers,¹² and peptosomes¹³ have been applied to bind and inhibit multivalent sugar-binding proteins. The development of 2-dimensional biomimetic nanomaterials has recently attracted enormous interest for different applications, like ion transport, biomimetic sieves, drug delivery and biosensing¹⁴. Lipids, polymers, and block co-polymers are the most reported building block for the preparation of such membrane mimetics.^{15,16} The natural tendency of phospholipids to self-assemble has been widely exploited to create “supported lipid bilayers”, where the lipids are self-assembled on a solid or polymeric substrate.^{17,18} Using this approach the obtained surface has been extensively used as a model for cell membrane and the introduction of synthetic glycans was also applied to study the behavior of carbohydrate-binding proteins to the membrane. Carbohydrate microarrays have recently become a powerful tool to study the multivalent interaction between sugars and proteins, due to the selectivity that governs this binding.¹⁹⁻²² These microarrays are prepared by depositing in ordered arrangement unmodified or modified carbohydrates, glycodendrimers, or glycopolymers to a solid surface, allowing the simultaneous analysis of a wide variety of carbohydrate-protein interactions.²³⁻²⁶

In the present work we develop a method to display sugars in structurally well-defined, free-floating two-dimensional (2D) arrays in a multivalent disposition at a

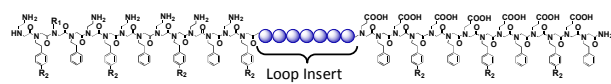
controlled density, taking advantage of the structure of peptoid nanosheets. Peptoids are a synthetic biomimetic polymer family composed of *N*-substituted glycine monomers.²⁷ We recently discovered that an opportunely designed sequence of alternating polar and non-polar peptoid monomers was able to self-assemble into highly stable, 2D nanosheets in water.²⁸⁻³⁰ Combining experimental results and molecular dynamics simulation, the atomic-resolution structure of this nanomaterial was determined, revealing a highly ordered self-assembled material.³¹ Different modifications of the polymer sequence have been investigated to study the properties of the resultant material,^{32,33} like the insertion of a hydrophilic domain to decorate the nanosheet with loops³⁴ or the insertion of photo-reactive crosslinking groups in the hydrophobic core to increase the stability of the nanosheets after photo-irradiation.³⁵ Peptoid nanosheets exhibit structural features similar to the cell membrane, like a hydrophobic core, a zwitterionic hydrophilic surface, a thickness of 3 nm and a length and width of hundreds of micrometers. Recently, the group of Chen reported a new peptoid-based material, that in addition to the characteristics just mentioned, resembles a cellular membrane also for its spontaneous assembly, the ability to self-repair and to respond to changes in Na⁺ concentration modifying its thickness.³⁶

Herein, we present a functionalized nanomaterial based on glycosylated peptoid nanosheets, able to mimic the cell surface and to specifically recognize proteins by multivalent interactions. An advantage in the use of peptoid is that contrary to standard polymers, their monomer sequence can be precisely controlled. This enables us to finely tune the nanosheet structure by introducing specific modifications. To create cell-surface mimetic nanosheets, a variety of carbohydrate units were covalently incorporated into the peptoid polymer using linkers of different lengths or within a loop-insert region (Table 1). The self-assembly of such peptoids resulted in the formation of engineered nanosheets, characterized by a homogeneously decorated surface with specific ligands for different macromolecules. The properties of these materials were then evaluated for their ability to recognize carbohydrate binding proteins. The multivalent lectins, Concanavalin A (ConA) and Wheat Germ Agglutinin (WGA), and Shiga toxin type 1 B subunit (Stx1B) were chosen to demonstrate the utility of this approach. A FRET binding assay was developed to enable high-throughput screening of a library of functionalized nanosheets and be able to determine selectivity and avidity of the different conjugates. We found that glycosylated peptoid nanosheets exhibit selective binding affinity to proteins by multivalent interactions as determined by fluorescence microscopy and Förster resonance energy transfer (FRET) studies.

RESULTS AND DISCUSSION

Synthesis of glycosylated peptoids. The ability of peptoids, a class of sequence-defined synthetic polymer, to

self-assemble into a 2D nanomaterial has been exploited to create a biofunctional free-floating material that mimics the cell surface. Peptoid nanosheets are formed by a hierarchical mechanism, which involves a first formation of an ordered monolayer at the air-water interface, followed by its irreversible collapse into a bilayer, due to a lateral compression.³⁰ The peptoid strands that form these supramolecular nanosheets are characterized by an alternating sequence of an aromatic monomers, *N*-(2-phenylethyl)glycine (Npe), and a polar, ionic monomer. The polar groups are distributed in two blocks, one anionic, composed of *N*-(2-carboxyethyl)glycine (Nce) monomers, and one cationic, with *N*-(2-aminoethyl)glycine (Nae) residues. We have developed an efficient strategy to engineer the peptoid strands to modulate the nanosheet features and the properties.³²⁻³⁵ Inserting short polar domains, composed of uncharged *N*-(2-methoxyethyl)glycine (Nme) residues, in the middle of the nanosheet forming peptoid sequence results in the display of loops on the exterior surface of the nanosheets to display functional groups of interest.³⁴ Recently, this strategy has been also exploited to incorporate a specific peptide on the loop for the molecular recognition of Alzheimer's disease serum.³⁷ Taking advantage of the modularity of the system, we inserted clickable alkyne sidechains into a loop sequence to enable the specific conjugation of ligands for surface display. Nanosheet-forming 28mer or 36mer peptoid sequences were modified with a single alkyne monomer with different linker lengths, or a series of hydrophilic monomers with an alkyne in the center to create a loop. In our previous study we observed that increasing the length of the inserted loop sequences influences the height and the roughness of the modified nanosheets proportionally, as monitored by atomic force microscopy (AFM) and X-ray powder diffraction (XRD).³⁴ Here, we introduced a hydrophilic loop domain composed of six residues of *N*-(2-methoxyethyl)glycine (Nme) residues with an *N*-propargylglycine residue in the middle (Table 1) to serve as the site of conjugation.



Peptoid	R1	R2	Loop	Sugar Displayed
1	--NH ₂	H	No Loop	-
2	--NH ₂	Ph	No Loop	-
3	--C≡CH	H	No Loop	-
4	--C≡CH	H	No Loop	-
5	--C≡CH	H	No Loop	Mannose
6	--C≡CH	H	No Loop	Mannose
7	--NH ₂	Ph	... (Nme) ₂ (Nme) ₃ ...	-
8	--NH ₂	Ph	... (Nme) ₂ (Nme) ₃ ...	Mannose
9	--NH ₂	Ph	... (Nme) ₂ (Nme) ₃ ...	<i>N</i> -Acetylglucosamine
10	--NH ₂	Ph	... (Nme) ₂ (Nme) ₃ ...	Galactose

Table 1. Structural modifications of the nanosheet-forming peptoid to display monosaccharides. Chemical structures of control peptoids **1-2** and functionalized peptoids bearing alkyne functional groups (**3-4** and **7**) for the conjugation of carbohydrates through copper-catalyzed azide-alkyne cycloaddition (CuAAC) **5-6** and **8-10**.

To introduce the saccharides onto the nanosheet surface, we designed both a pre- and a post-assembly conjugation approach (Figure 1). In the pre-assembly approach, free peptoids were firstly conjugated to carbohydrates, HPLC purified and then self-assembled. This approach has the advantage to precisely control the composition of the final nanosheet, permitting the study of ligand display density on the binding properties. Alternatively, to explore the possibility of creating combinatorial libraries of carbohydrate-functionalized nanosheets, a second approach was developed where un-functionalized alkyne nanosheets were first formed, and then the glycosylation reaction was performed *in situ* on the material. Using this pathway, it is possible to fractionate a single batch of nanosheets and attach a different carbohydrate to each portion (Figure 1 and Figure S1). In order to have a complete control on the composition of our nanomaterial and to be able to tune the density of the displayed sugars on the nanosheets surface, we primarily focus here on the pre-assembly conjugation approach.

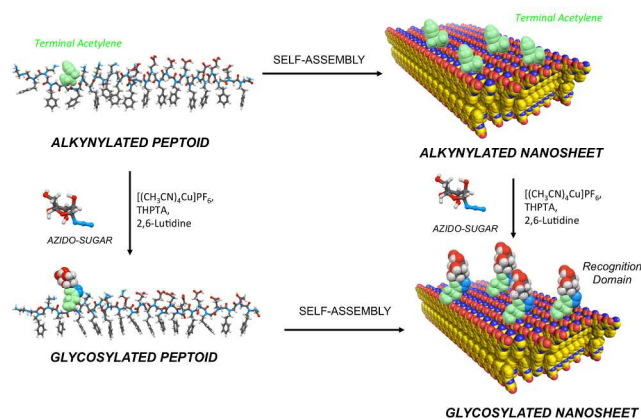


Figure 1. Scheme for the synthesis of glycosylated peptoid nanosheets. Starting from alkyne-functionalized peptoid, one route considers the glycosylation of the free peptoid followed by self-assembly into functionalized nanosheets (left). In the second route, nanosheets were first formed with the alkynylated peptoid followed by sugar conjugation (right).

Synthesis of glycosylated peptoid nanosheets. Click chemistry is a powerful tool to readily conjugate two molecules, and involves a 1,3-dipolar cycloaddition between an alkyne and an azide.³⁸ Depending on the alkyne, the reaction can be catalyzed by copper or can occur without any catalyst, a characteristic very appealing for the bio-conjugation in living systems. In previous works, click chemistry has been already utilized to cyclize peptoids on resin^{39,40} or to functionalize the polymer with estradiol and ferrocene⁴⁰ in an effort to develop therapeutics and biosensors based on peptoids. As an extension of this work, here we use the same approach to click bioactive molecules on the polymer to obtain functionalized peptoid nanosheets.

The standard nanosheet-forming 28mer peptoid was modified at the 26th position, replacing a polar Nae residue with an *N*-propargylglycine or an *N*-(4-pentynyl)glycine monomer (peptoids **3** and **4**, respectively) to study the impact of side chain linker length on the binding. These structures were designed to have two short linkers resulting in a spacing of 4 or 6 atoms between the peptoid backbone and the sugar (compounds **5** and **6**). We also designed constructs where the alkyne-containing monomer was flanked by several polar Nme monomers,³⁴ to display the sugar in the context of a flexible loop, perhaps making the sugars less sterically hindered. To compensate for the increased hydrophilicity generated by the loop and saccharide, it was necessary in certain cases to alternate on the hydrophobic core of the peptoid sequence *N*-(2-(4-biphenyl)ethyl)glycine and *N*-(2-phenethyl)glycine residues (e.g. peptoid **7**) in order to obtain good yields of nanosheet formation. Glycosylation reactions on the purified alkyne derivatives was performed on peptoids **3**, **4** and **7**. We took advantage of a recently reported procedure developed by the group of Fairbanks to synthesize peptide glycoconjugates directly in one-pot from native sugars.⁴¹ We first demonstrated

the approach by functionalizing the peptoids with mannose, which specifically binds the multivalent lectin protein ConA. Mannose was initially converted in the azido-derivative in the presence of 2-azido-1,3-dimethylimidazolium hexafluorophosphate, which acted as both activating agent for the anomeric hydroxylic group and source of azide. The reaction was performed in a mixture of D₂O and acetonitrile for 4 hours, using an excess of triethylamine. Without any purification of the azide-mannose derivative, the crude product was mixed with each of the purified alkyne-peptoids **3**, **4** or **7** in a solution of water and acetonitrile 1:1 (v/v), in the presence of tetrakis(acetonitrile)copper(I) hexafluorophosphate (TACP) as copper catalyst, 2,6-lutidine as base and tris-(hydroxypropyl)triazolymethylamine (THPTA), as stabilizing agent, affording overnight the desired glycosylated derivatives (Figure 2) in good yield. Each peptoid was then purified by HPLC and the final products were analyzed by analytical HPLC and MALDI mass spectrometry (See Supporting Information).

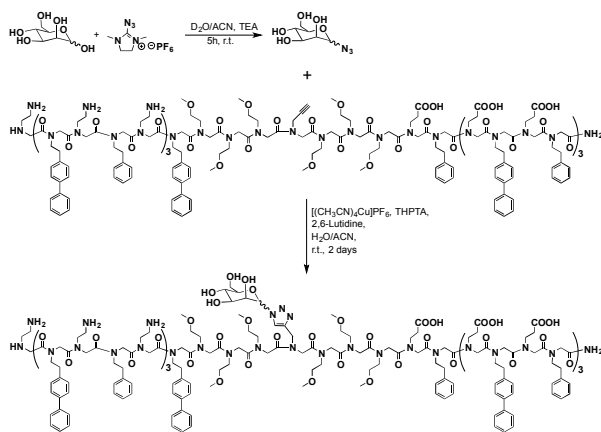


Figure 2. Cu catalyzed azide-alkyne cycloaddition reactions used to conjugate different monosaccharides to the alkyne-containing peptoid sequences.

A slightly different approach was followed to obtain more complex di- and trisaccharide conjugated glycopeptoids (**11-14**, Figure 3A). Here, we used a small loop in combination with a longer linker to the sugar unit. 36mer strands were modified by inserting one *N*-propargylglycine flanked by two Nme units in the middle of the peptoid oligomer sequence, resulting a 37mer (**S1**) and a 39mer (**S2**), respectively (Figure S2). These were used to conduct conjugation reactions with either 6-azido *N*-hexanoyl derivative of globotriosylamine (**18**), the natural ligand of Shiga toxin 1 subunit B (Stx1B), or β -D-lactosylamine (**17**) (used as control in the Stx1B binding study). Shiga toxin is an AB₅ toxin and is composed of two subunits. Subunit A is the bioactive part of the protein with enzymatic activity and subunit B which is a pentamer with 15 binding sites on one face for globotriaosylceramide to engage with cell surface receptors.⁴²⁻⁴⁴ In peptoids **12** and **14** displaying globotriose, the spacing between the pendant saccharide

and the peptoid backbone was designed such that there are at least 11 atoms between them to allow sufficient exposure on the hydrophilic exterior. In addition, based on the fully extended spacer length it was speculated that two saccharides in adjacent peptoid strands would be displayed to extend over two binding sites of Stx1B.⁴⁵ Indeed, the distance between binding sites on Shiga toxin is about 10 Å, while the distance between sugars (without a linker) on the peptoid nanosheets is expected to be around 9 Å (Figure S5C). The presence of a long linker allows additional mobility of the appended sugar, resulting in an increased distribution of the distances between sugars that could span between 0 and 20 Å. Globotriose with *N*-acyl aglycone at the reducing end has been shown to bind with Stx1B without losing affinity.⁴⁶ For this reason we used *N*-acyl sugar derivatives, which also facilitated their derivatization into clickable azido sugars. Azido sugar derivatives were made as shown in Figure 3B. First, glycosylamines (**15** and **16**) were made by reacting the corresponding reducing sugars with NH₄HCO₃ in aqueous ammonia followed by the acylation with *N*-hydroxysuccinimide activated 6-azidohexanoic acid (**19**).⁴⁷⁻⁴⁹

Alkylated peptoids (**S1** and **S2**) and azido sugar derivatives (**17** or **18**) were allowed to react in the presence of TACP and THPTA in DMF to afford the desired glycosylated derivatives (Figure 3A) in just two hours at room temperature. Each peptoid was then purified by HPLC to >90% purity to afford a 17-34% yield as analyzed by analytical HPLC and MALDI mass spectrometry.

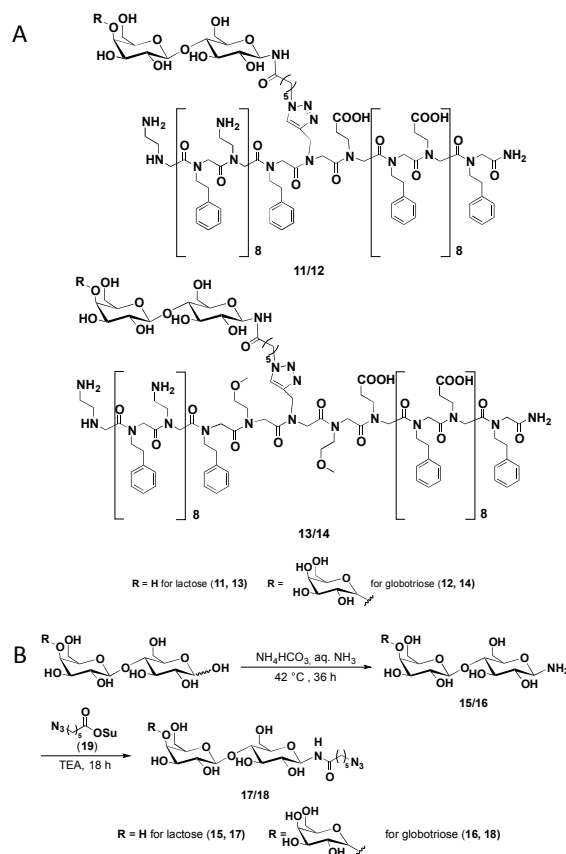


Figure 3. (A) Peptoid conjugates displaying globotriose and lactose. (B) Synthesis of 6-azido *N*-hexanoyl derivatives of β -D-lactosylamine and globotriosylamine.

Peptoid nanosheet assembly and characterization.

Glycosylated peptoids were then assembled into nanosheets. The formation of the nanosheets was analyzed by fluorescence microscopy (Figure 4) and SEM (Figure S3A-C), and their size and abundance was comparable with previously reported peptoid nanosheets.^{30, 34}

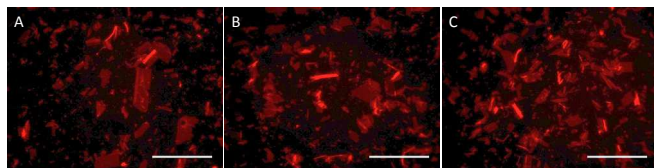


Figure 4. Fluorescence microscope images of glycosylated loop-peptoid nanosheets **8-10** functionalized with mannose (A), *N*-acetylglucosamine (B) and galactose (C). Scale bars represent 100 μ m.

Powder X-ray diffraction (XRD) was also performed to analyze the structural features of the material and in particular to assess the display of the loop on the functionalized nanosheets (Figure S3D-E). In our previous work^{28,34} we determined that XRD can directly provide information on the nanosheet thickness and chain-chain spacing. A characteristic peak at 4.6 \AA , is attributed to the peptoid inter-strand spacing, and was present in the XRD of all the glycosylated samples. Glycosylated peptoids **5** and **6** without loop showed a thickness of 3.0 and 3.1 nm, respectively, slightly higher than the control peptoid **1** (2.8 nm).³⁴ We previously showed that loops on peptoid nanosheets result in an increase in the material thickness. The same was observed here with the glycosylated loop-peptoid nanosheets. The nanosheets formed by mannose, *N*-acetylglucosamine and galactose derivatives (peptoid **8**, **9** and **10**) showed thicknesses in the range of 3.4 and 3.6 nm. In contrast nanosheets formed by peptoid **2** and

loop-peptoid **7** were 3.3 and 3.2 nm, respectively (Table 2). XRD data together with AFM measurements (Figure S4) indicates regular and ordered structures of the nanosheets, and are consistent with the display of the sugars on the nanosheet surface.

Protein binding to glycosylated nanosheets. Because of the high-density display of sugars in a planar format, the glycosylated peptoid nanosheets can be useful binders for multivalent threat agents such as toxins and viruses. As a model for the binding studies, the interaction between nanosheets and lectins, multivalent carbohydrate-binding proteins,⁵ were investigated. Specifically, mannose and *N*-acetylglucosamine are well-known ligands for Concanavalin A (ConA) and Wheat Germ Agglutinin (WGA), which are dimeric and tetrameric structures having 4 and 8 binding sites, respectively (Figure S5A and B).^{50,51} The shortest distance between binding sites for mannose and *N*-acetylglucosamine in ConA and WGA is approximately 7.0 and 1.1 nm, respectively. In the case of the glycosylated nanosheets, simple models suggest that the individual saccharide units are separated by a minimum distance of 0.9 nm. Due to the brick-like lattice of extended peptoid chains, there are two possible separations of sugars on the surface of glycosylated peptoid nanosheets that impact the binding site density (Figure S5C). To explore the performance of these materials, we next investigated the binding affinity of mannose (**8**) and *N*-acetylglucosamine (**9**) nanosheets for ConA and WGA using fluorescence microscopy and Förster resonance energy transfer (FRET).

Peptoid Derivative	Control Peptoid 2	Control Loop Peptoid 7	Mannose Peptoid 8	<i>N</i> -AcGlucosamine Peptoid 9	Galactose Peptoid 10
Nanosheets thickness from XRD	3.3 nm	3.2 nm	3.6 nm	3.4 nm	3.4 nm

Table 2. Thicknesses of glycosylated nanosheets as determined by XRD analysis.

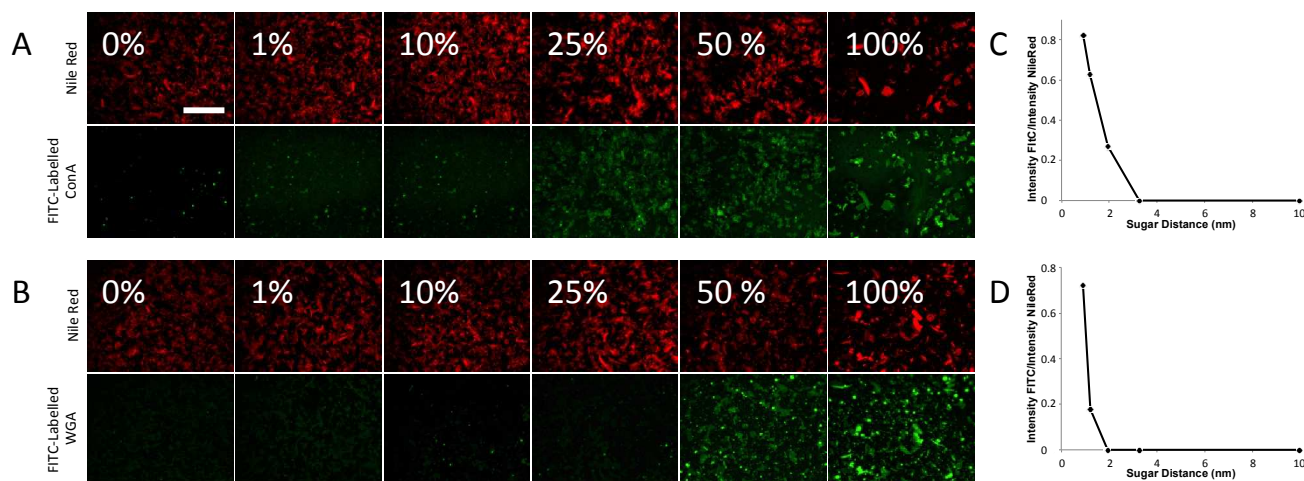


Figure 5. Lectin binding of glycosylated nanosheets as determined by fluorescence microscopy. Binding was evaluated as a function of sugar display density for (A) peptoid **8** and FITC-ConA and (B) for peptoid **9** and FITC-WGA. The material

was incubated respectively with FITC-ConA (A) or FITC-WGA (B) and the nanosheets were stained with Nile Red. Each image was collected using filters for both dyes: Nile Red (top A and B) and FITC (bottom A and B). Scale bar represents 100 μm . The fluorescence intensity ratio of FITC/Nile Red was used to quantitate the degree of binding in order to visualize the binding as a function of the approximate average sugar separation distance on the nanosheets for ConA (C) and WGA (D).

First, the interaction between mannosylated peptoid nanosheets and ConA was studied by using fluorescence microscopy. To interact with proteins of interest, sugar functionalities need to be displayed at the right distance to interact with multiple binding sites on the protein. To create nanosheets with different densities of sugar units on their surface, the nanosheets were prepared at various dilutions with un-functionalized peptoid **2**. This allowed us to correlate the degree of protein binding with the average separation distance of the sugars on the material surface.

Mannosylated peptoid nanosheets **5** and **6** (without loops and with short linkers) were mixed with fluorescently labeled FITC-ConA and incubated for 3 hours at room temperature before dialysis to remove unbound protein. The resultant material was then analyzed by fluorescence microscopy. The emission signal derived from these two peptoid nanosheets was very low, meaning that these conjugates were not able to bind specifically ConA (Figure S6). We believe that the lack of binding was caused by the inaccessibility of the carbohydrates on the material surface. For this reason, a different peptoid was designed to position the sugar in the center of a flexible hydrophilic loop (peptoid **8**). The added hydrophilicity of the polymer was compensated by using larger hydrophobic biphenyl residues, allowing the normal formation of the nanosheets. Engineering the peptoid in this way, the sugar moieties are likely more exposed on nanosheet surface and should be more readily accessible to the binding proteins. Peptoid nanosheets were prepared at different compositions (from 0% to 100%) of mannosylated peptoid **8** in a background of un-functionalized peptoid **2**. Although peptoid **8** is a 35mer and peptoid **2** is a 28mer, they have identical nanosheet-forming domains, and can co-assemble³⁴. In contrast to the peptoid nanosheets **5** and **6** without loop, a significant level of ConA binding was observed with the loop-nanosheets when the composition of **8** was higher than 25% (Figure 5A). To better understand the impact of ligand display density, we determined the intensity of the fluorescence signal detected from the FITC-ConA bound to the nanosheets as a function of the amount of glycosylated peptoid on the nanomaterial. We first calculated the average distances of sugar units displayed on the materials prepared with different dilutions (see S.I.). Because we assume that the distribution of sugar locations is stochastic, these distances are approximations of the average shortest possible distances between sites on the nanosheet. We then plot the intensity of the bound protein against the average sugar-to-sugar distance on the nanosheets surface (Figure 5C). We observed a dramatic increase in protein binding when the mannose units are less than 3 nm

apart from each other (corresponding to a 25% dilution of **8** into **2**). This spacing is the threshold distance to observe strong binding, suggesting cooperative behavior among multiple sugar units.

The same experiment was performed to investigate the ability of *N*-acetylglucosamine-functionalized peptoid nanosheets (**9**) to bind WGA. Peptoid nanosheets were self-assembled from peptoid **2** and **9** at different molar ratios and then incubated with WGA. As depicted in Figure 5B, significant protein binding was observed. Also, as observed for the mannosylated nanosheets, we observed a correlation between the carbohydrate surface-display distances and protein binding. Differently from before, here the threshold distance is slightly smaller, at 1.2 nm (corresponding to 50% of glycosylated peptoid), due to the smaller distance between the binding sites on WGA (Figure 5D). Indeed, the binding sites in ConA are 7.2 nm apart from each other, whereas in WGA they are only 1.4 nm apart. Thus, a higher density of *N*-acetylglucosamine is required in comparison to mannose to detect a binding event with WGA. These results are consistent with the expected trend of binding for ConA and WGA considering their inter-binding site distances.

This experiment shows the ability of peptoid nanosheets to display specific ligands on their surface, in particular when the cargo is exposed in the context of a hydrophilic loop. The distance between the peptoid backbone and the saccharides, or the flexibility of the loop play fundamental roles in the protein binding. Certainly, the steric accessibility of the sugars to the binding sites of the proteins is increased for nanosheets **8** and **9**, explaining the missed interaction of ConA with mannose derivatives **5** and **6**, which lack the loops.

To better quantitate the binding avidity of these glycosylated nanomaterials to bind proteins, we developed a homogeneous FRET binding assay. We employed BODIPY-FL C16, which can be inserted non-covalently into the nanosheet hydrophobic core to serve as a reporter upon binding to Alexa647-conjugated proteins. As a model system, biotinylated peptoid nanosheets were self-assembled with BODIPY-FL C16, and then Alexa647-conjugated streptavidin was added (Figure S7A). Upon protein binding the emission of BODIPY-FL C16 decreased and the emission at 675 nm increased (Figure S7C) indicating energy transfer between the fluorophores in close proximity to one another. As expected, this interaction was not observed in the case of un-functionalized peptoid nanosheets (Figure S7B). We next applied this assay format to the detection of ConA, WGA and Stx1B binding to glycosylated peptoid nanosheets. It is important to consider the size of the

protein in this type of screen. Indeed, the distance from a peptoid nanosheet to ConA and WGA could be as much as 9.5 and 5.5 nm, respectively (Figure 6A). However, since the proteins are labeled with multiple fluorophores, the average distance is on average significantly less. Because the FRET distance (R_0) of BODIPY-FL C16/Alexa647 pair is ~ 5 nm,⁵² a homogeneous FRET detection method should be effective to detect the binding of these proteins to the glycosylated peptoid nanosheets **8** and **9**.

As shown in Figure 6B, un-functionalized nanosheets **2** exhibited only BODIPY-FL C16 emission in the presence

of ConA and the photoluminescence (PL) spectra is essentially unchanged in the absence of ConA. In the case of the mannosylated peptoid nanosheets **8**, emission from Alexa647 at 675 nm becomes increasingly observable commensurate with a reduction in PL from the BODIPY-FL C16, due to ConA binding to the peptoid nanosheets and energy transfer. Similar results were observed upon the interaction of Alexa647-WGA with either *N*-acetyl-glucosamine peptoid nanosheets **9** or un-functionalized nanosheets **2**. As expected, FRET only occurred in the solution containing glycosylated nanosheets.

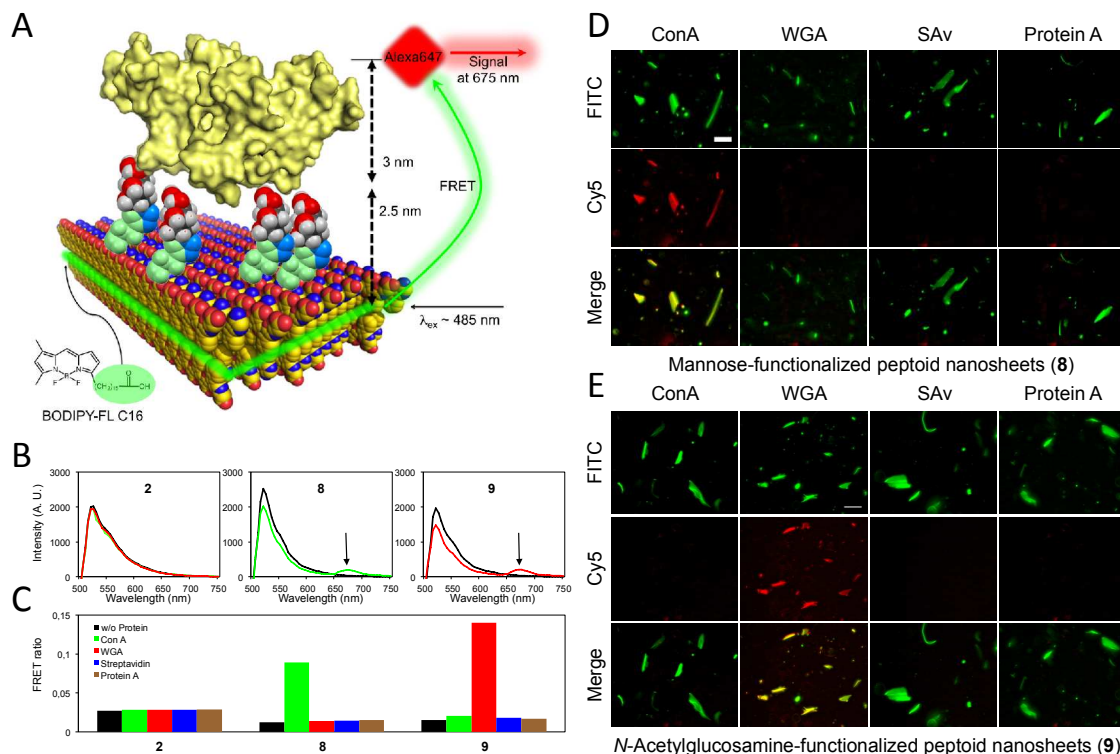


Figure 6. (A) Homogeneous FRET assay for the validation of protein binding to glycosylated peptoid nanosheets. (B) PL spectra of peptoid nanosheets **2**, **8** and **9** without (black) and with 250 nM Con A (green) and WGA (red). The arrows in the graphs highlight the signals of Alexa647 after the protein binding. All spectra were measured under the excitation wavelength at 485 nm. (C) FRET ratio (PL at 675 nm/ PL at 520 nm) of peptoid nanosheets **2**, **8** and **9** in the absence and presence of 250 nM ConA, WGA, streptavidin, and protein A. Fluorescence microscope images of glycosylated peptoid nanosheets **8** (D) and **9** (E) in the presence of ConA, WGA, streptavidin (SAv) or protein A. FITC and Cy5 channel are used for imaging BODIPY-FL incorporated into peptoid nanosheets and Alexa647 conjugated proteins, respectively. Scale bar represents 50 μ m.

The selectivity of the binding of peptoid nanosheets **8** and **9** was then investigated, by evaluating FRET signal against a panel of four proteins: ConA, WGA, streptavidin, and protein A (Figure 6C). First, we confirmed that un-functionalized peptoid nanosheets **2** have no binding affinity against any of the proteins. We found that the FRET ratio of glycosylated peptoid nanosheets **8** and **9** to ConA and WGA is 7 and 9 times higher than to the other proteins, meaning that the glycosylated peptoid nanosheets selectively bind the proteins. The selectivity

was also observed using fluorescence microscopy (Figure 6D-E). Only red emission from Alexa647-conjugated proteins was monitored in the glycosylated peptoid nanosheets **8** and **9** with ConA and WGA, respectively. The red emission is continuous with the green emission from BODIPY-FL C16 in the glycosylated peptoid nanosheets. Taken together, these experiments by the homogeneous FRET assay demonstrated that glycosylated peptoid nanosheets **8** and **9** have selective binding affinity to ConA and WGA.

Binding of Alexa647-conjugated Stx1B to peptoid nanosheets incorporating sequences **11**, **12**, **13**, or **14** were investigated using fluorescence microscopy. As shown in Figure 7B, only peptoid nanosheets displaying globotriose (**12** and **14**) show red emission. Conversely, peptoid nanosheets displaying lactose (**11** and **13**) do not show red emission. These observations clearly indicate that Stx1B was able to bind selectively to the globotriose nanosheets, relative to the disaccharide control. Interestingly, in this case we observed that the presence of a loop was not necessary for the protein binding. Indeed, using a longer linker (11 atoms between the peptoid backbone and the sugar instead of 4 and 6 for compounds **5-6**) globotriose was sufficiently exposed on the nanosheets surface for the binding of Stx1B.

Using the homogeneous FRET assay described for ConA and WGA we next studied the binding of Stx1B to peptoids **11-14**. As expected, lactose displaying peptoid nanosheets **11** and **13** did not show any emission from Alexa647, whereas globotriose displaying peptoids **12** and **14** showed significant emission at 675 nm, indicating binding (Figure 7A). We also evaluated the binding of **12** and **14** towards WGA, streptavidin, and protein A (*vide supra*). Nanosheets composed of conjugates **12** and **14** only bound to Stx1B and not to any other proteins tested (Figure S8). All these data suggest the selective binding of **12** and **14** to Stx1B. Moreover, the FRET assay (Figure S8) showed an increased binding of nanosheets **14** relative to **12**, meaning that even a small loop can improve the exposition of the sugars on the surface allowing higher protein recruitment.

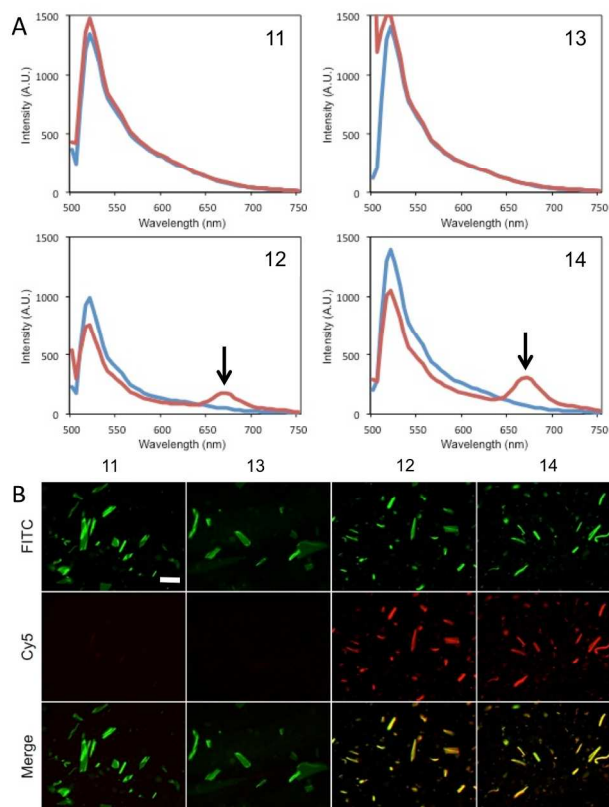


Figure 7. (A) FRET detection of Stx1B binding to lactose (**11**, **13**) and globotriose (**12**, **14**) peptoid nanosheets. (B) Fluorescence microscopic images of glycosylated peptoid nanosheets displaying lactose (**11**, **13**) and globotriose (**12**, **14**) incubated with labeled Stx1B. FITC and Cy5 channel are used for imaging BODIPY-FL incorporated into peptoid nanosheets and Alexa647 conjugated proteins, respectively. Scale bar represents 50 μm .

To determine the binding avidity of the functionalized nanosheets, we next explored the ability of free sugars to compete with the nanosheets for binding to the lectins. We focused on glycosylated peptoid nanosheets **9** for this study because of its higher binding efficiency for WGA than that of peptoid nanosheets **8** for ConA. For the competitive study, free *N*-acetylglucosamine was added at different concentrations to the solution containing the glycosylated peptoid nanosheets, prior to protein addition. The resulting binding curve is sigmoidal, with an inflection at $\sim 0.3 \mu\text{M}$ (Figure 8A). This suggests that the glycosylated peptoid nanosheets **9** interacts with the known binding site of WGA for *N*-acetylglucosamine. Because the IC_{50} of *N*-acetylglucosamine to WGA is $\sim 0.9 \mu\text{M}$,⁵⁰ there is a modest enhancement in binding due to the avidity resulting from multivalent display.

The cooperativity of this system was further studied by examining binding as a function of the protein concentration and of the sugar display density. This allows us to assess the binding avidity as a function of sugar display density.⁵³ The slope in the plot of FRET ratio versus the concentration of WGA becomes gradually steeper with the increasing percentage of **9** in the peptoid nanosheets, indicating that the binding affinity to WGA is enhanced when the density of *N*-acetylglucosamine on the surface of the nanosheets is higher. This is consistent with previous reports,⁵⁴ where multivalent guest binding is significantly enhanced with a high density of targets. Thus, glycosylated peptoid nanosheets can be used as multivalent scaffolds to interact with target proteins and varying the display of the sugars we can tune the biological response.

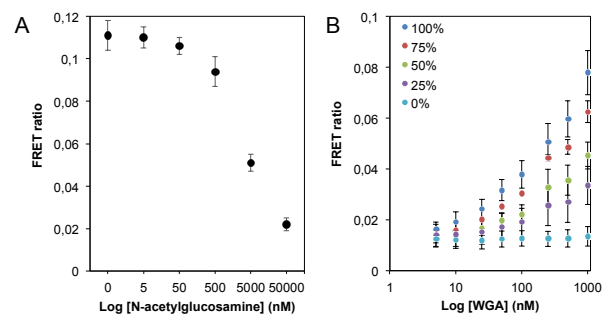


Figure 8. (A) Competitive inhibition experiment with free *N*-acetylglucosamine using the FRET assay to determine the IC_{50} value for glycosylated nanosheets **9** for WGA. The FRET ratio of WGA and glycosylated peptoid nanosheets **9** (PL at 675nm/PL at 520nm) was measured at various concentrations of free *N*-acetylglucosamine. (B) Titration curve of the FRET ratio (PL at 675nm/PL at 520nm) varying the concentration of WGA and using glycosylated

nanosheets with different compositions of peptoid **9** diluted with peptoid **2**.

CONCLUSION

Inspired by nature, we engineered the surface of peptoid nanosheets to mimic some of the properties of the cellular membrane to interact with multivalent proteins. Taking advantage of the known affinity of many proteins for carbohydrates, we functionalized the surface of peptoid nanosheets with a variety of simple sugars. Using copper-catalyzed azide-alkyne cycloaddition a library of glycopeptoid conjugates was synthesized, establishing a versatile and facile synthetic procedure. The saccharide unit was appended to the middle of a hydrophilic loop domain on the peptoid strand or using a linker to allow the display of the sugar on the material. The subsequent formation of glycosylated peptoid nanosheets was demonstrated by fluorescence microscopy, SEM and XRD. The display of the sugars within the flexible loop context was critical for the productive and selective interaction with the lectins ConA and WGA. To further analyze and quantitate the multivalent properties of the material, a FRET binding assay was developed. Using two different dyes, BODIPY-FL C16 incorporated into the nanosheets and Alexa647 labeled proteins, energy transfer from BODIPY-FL C16 to Alexa647 could be used to monitor protein binding. Binding to ConA and WGA was observed only with the glycosylated loop-nanosheets, in comparison to unfunctionalized peptoid nanosheets, confirming the efficient interaction between glycosylated nanosheets and multivalent proteins. The binding was shown to be specific against a small panel of proteins, and competitive with free sugar. Binding avidity was also shown to depend on the display density of sugars on the sheet surface, where the sugar ligands can be close enough to achieve enhanced avidity through multivalent interactions. Shiga toxin subunit B binding to globotriose-functionalized nanosheets was also demonstrated.

In summary, a convenient method has been developed to display mono-, di- and tri-saccharides at controlled densities on the surface of freely soluble peptoid nanosheets. These constructs are simple mimetics of the cell surface that can effectively bind the lectins Con A and WGA, as well as the clinically relevant Shiga toxin subunit B. Such constructs offer the potential to selectively bind to other multivalent proteins, or potentially intact viruses or cells. The homogeneous FRET assay is amenable to high-throughput screening, allowing combinatorial libraries of multivalent 2D nanomaterials to be screened for selective protein binding. Such materials are poised to impact the discovery of molecular recognition elements for sensors, as therapeutics and as materials for bioremediation of threat agents.

MATERIALS AND METHODS

All reagents and solvents used for the peptoid synthesis and for the binding studies were purchased from commercial sources and used without further purification.

General procedure for the synthesis of monosaccharide peptoid conjugates. Mannose (1.73 mg, 2 eq.) and triethylamine (6.71 μ L, 10 eq.) were dissolved in 80 μ L of D₂O and the solution was cooled to 0 °C in an ice bath. 2-Azido-1,3-dimethylimidazolium hexafluorophosphate (2.74 mg, 2 eq.) was dissolved in 20 μ L of acetonitrile and added to the mannose solution. The mixture was then incubated for 5 hours at room temperature. Purified peptoid **8** (25.0 mg, 1 eq.) was dissolved in 500 μ L of acetonitrile/water 1:1 and 2,6-lutidine (84 μ L, 150 eq.) was added. Then, the azide-derivative mannose solution (without further modification), THPTA (10.5 mg, 5 eq.) and tetrakis(acetonitrile)copper(I) hexafluorophosphate (8.96 mg, 5 eq.) were added to the peptoid solution and the reaction mixture was stirred overnight at room temperature.

After that time, the solvent was evaporated and the crude peptoid was purified by reverse phase preparative HPLC. Eluent: A (0.1% TFA, v/v in water) and B (0.1% TFA, v/v in acetonitrile); gradient: sample was run at 15 mL/min with a gradient of 42-70% B in 100 minutes and UV detection at 214 nm. After lyophilization from acetonitrile/water (1:1, v/v), the product was obtained as a white powder. Products were characterized by MALDI-TOF and purity confirmed by reverse phase analytical HPLC using a linear gradient of 20-80% acetonitrile and water containing 0.1% TFA within 30 min at 1 mL/min flow rate and UV detection at 214 nm. For peptoid **4** and **5**, the gradient used for the purification was 35-55% in 80 minutes.

The same procedure was adopted to functionalize peptoids with galactose and *N*-acetylglucosamine. In the synthesis of azido derivative *N*-acetylglucosamine, the procedure was slight modified as described previously. After 5 hours of incubation, the solution was acidified to pH 2 using 1M HCl and then neutralized to pH 7 by adding saturated NaHCO₃ solution, to avoid the formation of oxazoline derivative.

Synthesis of 6-azido *N*-hexanoyl derivatives β -D-lactosylamine (17**) and globotriosylamine (**18**).** A solution of NH₄HCO₃ (1 mg, 12.6 μ mol) in 100 μ L 15 M aq. NH₃ (Sigma Aldrich) was mixed with either β -D-lactose (Alfa-Aesar) or globotriose (Carbosynth Ltd, UK and LC Scientific Inc. Canada) (10 μ mol for both) and stirred at 42 °C for 36 h. The crude mixture was diluted with 400 μ L of water and lyophilized. MeOH (2 mL) was added to the resulting white residue and the solvent was evaporated under reduced pressure to remove bicarbonate. This procedure was repeated five more times until the solution was at neutral pH as monitored by indicator paper. The residue was dissolved in water and lyophilized to give a white powder and was carried to the acylation step immediately. Crude glycosylamine (**15** or **16**) (10 μ mol) in water (30 μ L) was cooled to 0 °C and added to DMF (200 μ L) in an ice bath, followed by addition of 6-azidohexanoic acid succinimidyl ester (**19**) (10 μ mol, 1 eq.) and triethylamine (2 μ L, 14 μ mol, 1.4 eq.). The mixture was stirred at room temperature overnight. Another portion of **19** (1 μ L, 7 μ mol) was then added and stirred for an additional 2 days. The ester **19** was not

added at more than 2 times equivalents in order to minimize the undesired click product potentially formed by hydrolyzed 6-azidohexanoic acid in the subsequent step. DMF was removed *in vacuo* to dryness by co-evaporating with MeOH. The residue was carefully washed three times with DCM, dissolved in water and lyophilized to obtain **17** (5 mg) and **18** (6 mg) as a white solid and carried to the next step without further purification. **15** HRMS (ESI) m/z calcd for $C_{12}H_{24}NO_{10}$ (M+H)⁺ 342.13, found 342.09, **16** HRMS (ESI-TOF) m/z calcd for $C_{18}H_{34}NO_{15}$ (M+H)⁺ 504.1923, found 504.1930, **17** HRMS (ESI-TOF) m/z calcd for $C_{18}H_{33}N_4O_{11}$ (M+H)⁺ 481.2140, found 481.2138, **18** HRMS (ESI-TOF) m/z calcd for $C_{24}H_{43}N_4O_{16}$ (M+H)⁺ 643.2674, found 643.2676.

Synthesis of lactose and globotriose peptoids. To a solution of alkylated peptoid (**S1** or **S2**, see Figure S2) (0.8 μ mol, based on molecular weight of the TFA salt) in degassed DMF (400 μ L) was added the azido-sugars **17** or **18** (2.33 μ mol, 3 eq.) in water (70 μ L), TACP (6 μ mol, 6 eq.) and THPTA (6 μ mol, 6 eq.), purged with nitrogen and stirred for 2 h at room temperature. DMF was removed *in vacuo* to dryness. Residue was dissolved in 0.1 M Na₂EDTA (aq.):acetonitrile (7:3) and purification was carried out by reverse phase HPLC on a 250 \times 21.2 mm, 10 μ m, 300 \AA , Jupiter preparative C18 column using a linear gradient of 30-80% acetonitrile in water containing 0.1% TFA (v/v) over 60 min at 10 mL/min flow rate and UV detection at 214 nm. After lyophilization, the product was obtained as a white powder. Products were analyzed by MALDI-TOF and purity confirmed by reverse phase analytical HPLC (150 mm \times 4.6 mm, 5 μ m, Vydac 218TP C18 column) using a linear gradient of 5-95% acetonitrile and water containing 0.1% TFA (v/v) over 15 min at 1 mL/min flow rate and UV detection at 214 nm. See SI for characterization data.

Formation of peptoid nanosheets. Peptoid nanosheets were prepared as described previously.^{30,34} Briefly, purified peptoids were dissolved in a 2:1 (v/v) mixture of DMSO/water in a 2 mM stock solution. In a 4 mL (1 dram) cylindrical glass vial, a 20 μ M peptoid solution was prepared in 10 mM Tris-HCl buffer, pH 8, with a final volume of 500 μ L. The solution was gently mixed and then rotated from vertical to horizontal at room temperature using a custom-built device that rotates the vial every 30 min.³⁰

Protein binding via fluorescence microscopy. Experiments with FITC-ConA were performed using the following buffer condition: 10 mM Tris, 150 mM NaCl, 0.01% Casein hydrolysate, 1 mM MnCl₂ and 1 mM CaCl₂, pH 7.0. Experiments with FITC-WGA were performed using the following buffer condition: 10 mM Tris, 150 mM NaCl and 0.01% Casein hydrolysate, pH 7.0. 100 μ L of peptoid nanosheets were gently mixed 100 μ L of FITC-protein (final protein concentration 0.5 μ M) and incubated at room temperature for 3 hours in the dark. At that time, the nanosheets were dialyzed against the experiment buffer for 3 hours in 1 mL float-a-lyzer G2, Spectra/Por (300 kD MWCO for ConA and 100 kD MWCO for WGA) to remove the excess of unbound protein. 2 μ L of nanosheets were deposited on 1.5% agarose

gel, after complete adsorption 2 μ L of Nile Red 2 μ M was added and then the nanomaterial was imaged. Optical imaging of nanosheets was performed under epifluorescence illumination with an Olympus IX81 inverted microscope, fitted with a Hamamatsu Orca CCD camera.

Homogeneous FRET binding assay for detecting protein-nanosheet interactions. For the homogeneous FRET assay to validate protein binding to loop-functionalized peptoid nanosheets, nanosheet-forming solution with 5 μ M BODIPY-FL C16 was self-assembled by rocking machine (rocking number was \sim 250 and the waiting time per rock was 10 sec) as previously reported.³⁰ Then, the BODIPY-FL C16 incorporated peptoid nanosheets were mixed with the Alexa647-conjugated protein solutions at the following final concentration: 10 mM nanosheets, 2.5 mM BODIPY-FL C16, and 250 nM Alexa-conjugated proteins in 25 mM phosphate buffer, 150 mM NaCl, pH 7.4. In case of the competitive study in Figure 8, *N*-acetylglucosamine monomer was added before the addition of protein-containing solution to peptoid nanosheet. All fluorescence spectra were obtained using plate-reader under the excitation wavelength at 485 nm.

ASSOCIATED CONTENT

Supporting Information

The Supporting Information is available free of charge on the ACS Publications website at DOI: (insert link here) Glycofunctionalized peptoid nanosheet synthesis and characterization, fluorescence microscopy, homogeneous FRET-based binding assay, binding selectivity assays.

AUTHOR INFORMATION

Corresponding Author

*E-mail: rnzuckermann@lbl.gov.

Author Contributions

The manuscript was written through contributions of all authors. All authors have given approval to the final version of the manuscript.

ACKNOWLEDGMENT

This project was funded by the Defense Threat Reduction Agency under contract no. DTRA10027-15875 and the DARPA Fold F(x) program. The work was conducted at the Molecular Foundry with support from the Advanced Light Source at Lawrence Berkeley National Laboratory, both of which are supported by the Office of Science, Office of Basic Energy Sciences, U.S. Department of Energy under contract no. DEAC02-05CH11231. J. H. Kim acknowledges the National Research Foundation (NRF) for supporting his postdoctoral fellowship granted by the Korea government (NRF-2016R1A6A3A03007606).

REFERENCES

1. Fasting, C.; Schalley, C. A.; Weber, M.; Seitz, O.; Hecht, S.; Kokscha, B.; Dornedde, J.; Graf, C.; Knapp, E.-W.; Haag, R., Multivalency as a Chemical Organization and Action Principle. *Angew. Chem. Int. Ed.* **2012**, *51*, 10472-10498.
2. Mammen, M.; Choi, S.-K.; Whitesides, G. M., Polyvalent Interactions in Biological Systems: Implications for Design and Use of Multivalent Ligands and Inhibitors. *Angew. Chem. Int. Ed.* **1998**, *37*, 2754-2794.
3. Grove, J.; Marsh, M., The Cell Biology of Receptor-mediated Virus Entry. *J. Cell. Biol.* **2011**, *195*, 1071-1082.
4. Pizarro-Cerdá, J.; Cossart, P., Bacterial Adhesion and Entry into Host Cells. *Cell* **2006**, *124*, 715-727.
5. Wittmann, V.; Pieters, R. J., Bridging Lectin Binding Sites by Multivalent Carbohydrates. *Chem. Soc. Rev.* **2013**, *42*, 4492-4503.
6. Bonduelle, C.; Lecommandoux, S., Synthetic Glycopolypeptides as Biomimetic Analogues of Natural Glycoproteins. *Biomacromol.* **2013**, *14*, 2973-2983.
7. Gestwicki, J. E.; Cairo, C. W.; Strong, L. E.; Oetjen, K. A.; Kiessling, L. L., Influencing Receptor-Ligand Binding Mechanisms with Multivalent Ligand Architecture. *J. Am. Chem. Soc.* **2002**, *124*, 14922-14933.
8. Maier, M. A.; Yannopoulos, C. G.; Mohamed, N.; Roland, A.; Fritz, H.; Mohan, V.; Just, G.; Manoharan, M., Synthesis of Antisense Oligonucleotides Conjugated to a Multivalent Carbohydrate Cluster for Cellular Targeting. *Bioconj. Chem.* **2003**, *14*, 18-29.
9. Branson, T. R.; McAllister, T. E.; Garcia-Hartjes, J.; Fascione, M. A.; Ross, J. F.; Warriner, S. L.; Wennekes, T.; Zuilhof, H.; Turnbull, W. B., A Protein-Based Pentavalent Inhibitor of the Cholera Toxin B-Subunit. *Angew. Chem. Int. Ed.* **2014**, *53*, 8323-8327.
10. Muñoz, A.; Sigwalt, D.; Illescas, B. M.; Luczkowiak, J.; Rodríguez-Pérez, L.; Nierengarten, I.; Holler, M.; Remy, J.-S.; Buffet, K.; Vincent, S. P.; Rojo, J.; Delgado, R.; Nierengarten, J.-F.; Martín, N., Synthesis of Giant Globular Multivalent Glycofullerenes as Potent Inhibitors in a Model of Ebola Virus Infection. *Nat. Chem.* **2016**, *8*, 50-57.
11. Vincent, S. P.; Buffet, K.; Nierengarten, I.; Imberty, A.; Nierengarten, J.-F., Biologically Active Heteroglycoclusters Constructed on a Pillar[5]arene-Containing [2]Rotaxane Scaffold. *Chemistry* **2016**, *22*, 88-92.
12. Pati, D.; Shaikh, A. Y.; Das, S.; Nareddy, P. K.; Swamy, M. J.; Hotha, S.; Gupta, S. S., Controlled Synthesis of O-Glycopolypeptide Polymers and Their Molecular Recognition by Lectins. *Biomacromol.* **2012**, *13*, 1287-1295.
13. Huang, J.; Bonduelle, C.; Thévenot, J.; Lecommandoux, S.; Heise, A., Biologically Active Polymersomes from Amphiphilic Glycopeptides. *J. Am. Chem. Soc.* **2012**, *134*, 119-122.
14. Mu, P.; Zhou, G.; Chen, C.-L., 2D Nanomaterials Assembled from Sequence-defined Molecules. *Nano-Struct. Nano-Obj.* **2017**. <https://doi.org/10.1016/j.nanoso.2017.09.010>.
15. Zhang, X.; Tanner, P.; Graff, A.; Palivan, C. G.; Meier, W., Mimicking the Cell Membrane with Block Copolymer Membranes. *J. Polym. Sci. A* **2012**, *50*, 2293-2318.
16. Puri, A.; Blumenthal, R., Polymeric Lipid Assemblies as Novel Theranostic Tools. *Acc. Chem. Res.* **2011**, *44*, 1071-1079.
17. Tanaka, M.; Sackmann, E., Polymer-Supported Membranes as Models of the Cell Surface. *Nature* **2005**, *437*, 656-663.
18. Groves, J. T.; Boxer, S. G., Micropattern Formation in Supported Lipid Membranes. *Acc. Chem. Res.* **2002**, *35*, 149-157.
19. Liang, P.-H.; Wu, C.-Y.; Greenberg, W. A.; Wong, C.-H., Glycan Arrays: Biological and Medical Applications. *Curr. Op. Struct. Biol.* **2008**, *12*, 86-92.
20. Oyelaran, O.; Gildersleeve, J. C., Glycan Arrays: Recent Advances and Future Challenges. *Curr. Op. Struct. Biol.* **2009**, *13*, 406-413.
21. Park, S.; Gildersleeve, J. C.; Blixt, O.; Shin, I., Carbohydrate microarrays. *Chem. Soc. Rev.* **2013**, *42*, 4310-4326.
22. Paulson, J. C.; Blixt, O.; Collins, B. E., Sweet spots in functional glycomics. *Nat. Chem. Biol.* **2006**, *2*, 238-248.
23. Branderhorst, H. M.; Ruijtenbeek, R.; Liskamp, R. M. J.; Pieters, R. J., Multivalent Carbohydrate Recognition on a Glycodendrimer-Functionalized Flow-Through Chip. *ChemBioChem* **2008**, *9*, 1836-1844.
24. Park, S.; Lee, M.-R.; Shin, I., Chemical Tools for Functional Studies of Glycans. *Chem. Soc. Rev.* **2008**, *37*, 1579-1591.
25. Huang, M. L.; Cohen, M.; Fisher, C. J.; Schooley, R. T.; Gagneux, P.; Godula, K., Determination of Receptor Specificities for Whole Influenza Viruses Using Multivalent Glycan Arrays. *Chem. Commun.* **2015**, *51*, 5326-5329.
26. Godula, K.; Bertozzi, C. R., Density Variant Glycan Microarray for Evaluating Cross-Linking of Mucin-like Glycoconjugates by Lectins. *J. Am. Chem. Soc.* **2012**, *134*, 15732-15742.
27. Sun, J.; Zuckermann, R. N., Peptoid Polymers: A Highly Designable Bioinspired Material. *ACS Nano* **2013**, *7*, 4715-4732.
28. Nam, K. T.; Shelby, S. A.; Choi, P. H.; Marciel, A. B.; Chen, R.; Tan, L.; Chu, T. K.; Mesch, R. A.; Lee, B.-C.; Connolly, M. D.; Kisielowski, C.; Zuckermann, R. N., Free-Floating Ultrathin Two-Dimensional Crystals from Sequence-Specific Peptoid Polymers. *Nat. Mater.* **2010**, *9*, 454-460.
29. Robertson, E. J.; Battigelli, A.; Proulx, C.; Mannige, R. V.; Haxton, T. K.; Yun, L.; Whitlam, S.; Zuckermann, R. N., Design, Synthesis, Assembly, and Engineering of Peptoid Nanosheets. *Acc. Chem. Res.* **2016**, *49*, 379-389.

30. Sanii, B.; Kudirka, R.; Cho, A.; Venkateswaran, N.; Olivier, G. K.; Olson, A. M.; Tran, H.; Harada, R. M.; Tan, L.; Zuckermann, R. N., Shaken, Not Stirred: Collapsing a Peptoid Monolayer To Produce Free-Floating, Stable Nanosheets. *J. Am. Chem. Soc.* **2011**, *133*, 20808-20815.
31. Mannige, R. V.; Haxton, T. K.; Proulx, C.; Robertson, E. J.; Battigelli, A.; Butterfoss, G. L.; Zuckermann, R. N.; Whitelam, S., Peptoid Nanosheets Exhibit a New Secondary-Structure Motif. *Nature* **2015**, *526*, 415-420.
32. Robertson, E. J.; Proulx, C.; Su, J. K.; Garcia, R. L.; Yoo, S.; Nehls, E. M.; Connolly, M. D.; Taravati, L.; Zuckermann, R. N., Molecular Engineering of the Peptoid Nanosheet Hydrophobic Core. *Langmuir* **2016**, *32*, 11946-11957.
33. Robertson, E. J.; Nehls, E. M.; Zuckermann, R. N., Structure-Rheology Relationship in Nanosheet-Forming Peptoid Monolayers. *Langmuir* **2016**, *32*, 12146-12158.
34. Olivier, G. K.; Cho, A.; Sanii, B.; Connolly, M. D.; Tran, H.; Zuckermann, R. N., Antibody-Mimetic Peptoid Nanosheets for Molecular Recognition. *ACS Nano* **2013**, *7*, 9276-9286.
35. Flood, D.; Proulx, C.; Robertson, E. J.; Battigelli, A.; Wang, S.; Schwartzberg, A. M.; Zuckermann, R. N., Improved Chemical and Mechanical Stability of Peptoid Nanosheets by Photo-Crosslinking the Hydrophobic Core. *Chem. Commun.* **2016**, *52*, 4753-4756.
36. Jin, H.; Jiao, F.; Daily, M. D.; Chen, Y.; Yan, F.; Ding, Y.-H.; Zhang, X.; Robertson, E. J.; Baer, M. D.; Chen, C.-L., Highly Stable and Self-Repairing Membrane-Mimetic 2D Nanomaterials Assembled from Lipid-Like Peptoids. *Nat. Commun.* **2016**, *7*, 12252.
37. Zhu, L.; Zhao, Z.; Cheng, P.; He, Z.; Cheng, Z.; Peng, J.; Wang, H.; Wang, C.; Yang, Y.; Hu, Z., Antibody-Mimetic Peptoid Nanosheet for Label-Free Serum-Based Diagnosis of Alzheimer's Disease. *Adv. Mater.* **2017**, *29*, 1700057-n/a.
38. Kolb, H. C.; Finn, M. G.; Sharpless, K. B., Click Chemistry: Diverse Chemical Function from a Few Good Reactions. *Angew. Chem. Int. Ed.* **2001**, *40*, 2004-2021.
39. Jagasia, R.; Holub, J. M.; Bollinger, M.; Kirshenbaum, K.; Finn, M. G., Peptide Cyclization and Cyclodimerization by CuI-Mediated Azide-Alkyne Cycloaddition. *J. Org. Chem.* **2009**, *74*, 2964-2974.
40. Holub, J. M.; Jang, H.; Kirshenbaum, K., Clickity-Click: Highly Functionalized Peptoid Oligomers Generated by Sequential Conjugation Reactions on Solid-Phase Support. *Org. Biomol. Chem.* **2006**, *4*, 1497-1502.
41. Lim, D.; Brimble, M. A.; Kowalczyk, R.; Watson, A. J. A.; Fairbanks, A. J., Protecting-Group-Free One-Pot Synthesis of Glycoconjugates Directly from Reducing Sugars. *Angew. Chem. Int. Ed.* **2014**, *53*, 11907-11911.
42. Melton-Celsa, A. R., Shiga Toxin (Stx) Classification, Structure, and Function. *Microbiol. Spectrum* **2014**, *2*, 10.1128/microbiolspec.EHEC-0024-2013.
43. Merritt, E. A.; Hol, W. G. J., AB₅ toxins. *Curr. Op. Struct. Biol.* **1995**, *5*, 165-171.
44. Jacewicz, M.; Clausen, H.; Nudelman, E.; Donohue-Rolfe, A.; Keusch, G. T., Pathogenesis of Shigella Diarrhea. XI. Isolation of a Shigella Toxin-Binding Glycolipid from Rabbit Jejunum and HeLa Cells and its Identification as Globotriaosylceramide. *J. Exp. Med.* **1986**, *163*, 1391-1404.
45. Kitov, P. I.; Sadowska, J. M.; Mulvey, G.; Armstrong, G. D.; Ling, H.; Pannu, N. S.; Read, R. J.; Bundle, D. R., Shiga-like toxins are neutralized by tailored multivalent carbohydrate ligands. *Nature* **2000**, *403*, 669-672.
46. Kitova, E. N.; Kitov, P. I.; Paszkiewicz, E.; Kim, J.; Mulvey, G. L.; Armstrong, G. D.; Bundle, D. R.; Klassen, J. S., Affinities of Shiga toxins 1 and 2 for Univalent and Oligovalent Pk-Trisaccharide Analogs Measured by Electrospray Ionization mass spectrometry. *Glycobiol.* **2007**, *17*, 1127-1137.
47. Lubineau, A.; Augé, J.; Drouillard, B., Improved Synthesis of Glycosylamines and a Straightforward Preparation of N-Acylglycosylamines as Carbohydrate-Based Detergents. *Carbohydr. Res.* **1995**, *266*, 211-219.
48. Likhoshesterov, L. M.; Novikova, O. S.; Yamskov, I. A.; Piskarev, V. E., Synthesis of N-Glycyl-β-Glycopyranosylamines, Human Milk Fucooligosaccharide Derivatives. *Russ. Chem. Bull.* **2012**, *61*, 1816-1821.
49. Grandjean, C.; Boutonnier, A.; Guerreiro, C.; Fournier, J.-M.; Mulard, L. A., On the Preparation of Carbohydrate-Protein Conjugates Using the Traceless Staudinger Ligation. *J. Org. Chem.* **2005**, *70*, 7123-7132.
50. Schwefel, D.; Maierhofer, C.; Beck, J. G.; Seeberger, S.; Diederichs, K.; Möller, H. M.; Welte, W.; Wittmann, V., Structural Basis of Multivalent Binding to Wheat Germ Agglutinin. *J. Am. Chem. Soc.* **2010**, *132*, 8704-8719.
51. Kanellopoulos, P. N.; Pavlou, K.; Perrakis, A.; Agianian, B.; Vorgias, C. E.; Mavrommatis, C.; Soufi, M.; Tucker, P. A.; Hamodrakas, S. J., The Crystal Structure of the Complexes of Concanavalin A with 4'-Nitrophenyl-α-d-mannopyranoside and 4'-Nitrophenyl-α-d-glucopyranoside. *J. Struct. Biol.* **1996**, *116*, 345-355.
52. Mazouchi, A.; Zhang, Z.; Bahram, A.; Gomes, G.-N.; Lin, H.; Song, J.; Chan, Hue S.; Forman-Kay, Julie D.; Gradinaru, Claudiu C., Conformations of a Metastable SH₃ Domain Characterized by smFRET and an Excluded-Volume Polymer Model. *Biophys. J.* **2016**, *110*, 1510-1522.
53. Guo, Y.; Sakonsinsiri, C.; Nehlmeier, I.; Fascione, M. A.; Zhang, H.; Wang, W.; Pöhlmann, S.; Turnbull, W. B.; Zhou, D., Compact, Polyvalent Mannose Quantum Dots as Sensitive, Ratiometric FRET Probes for Multivalent Protein-Ligand Interactions. *Angew. Chem. Int. Ed.* **2016**, *55*, 4738-4742.

- 1 54. Martinez-Veracoechea, F. J.; Frenkel, D., Designing
2 Super Selectivity in Multivalent Nanoparticle
3 Binding. *Proc. Natl. Acad. Sci. U.S.A.* **2011**, *108*,
4 10963-10968.
5
6
7
8
9
10
11
12
13
14
15
16
17
18
19
20
21
22
23
24
25
26
27
28
29
30
31
32
33
34
35
36
37
38
39
40
41
42
43
44
45
46
47
48
49
50
51
52
53
54
55
56
57
58
59
60

TOC Graphic

